Supporting Information For

Rapid electrodeposition of gold-Prussian blue nanocomposite of ultrahigh electroactivity for dual-potential amperometric biosensing of uric acid

Wen Wang,[a] Cong Qin,[a] Qingji Xie,*[,a] Xiaoli Qin,[a] Long Chao,[a] Yi Huang,[a] Mengzhen Dai,[a] Chao Chen,*[,a] Jianying Huang,[a] Jiming Hu[b]

[a]*Key Laboratory of Chemical Biology & Traditional Chinese Medicine Research (Ministry of Education of China), College of Chemistry and Chemical Engineering, Hunan Normal University, Changsha 410081, China. E–mail: xieqj@hunnu.edu.cn; chenchao840103@163.com. Tel./Fax: +86 731 88872046*

[b]*Key Laboratory of Analytical Chemistry for Biology and Medicine (Ministry of Education of China), Wuhan University, Wuhan 430072, China*

Contents

Quantification of the enzymatic activity

For the evaluation of ESA_n, the procedures were (1) an amperometric working curve was drawn to correlate the H_2O_2 concentration with the static current for reduction of H_2O_2 on an $(Au\text{-}PB)_{REd}$/Au disk electrode at -0.05 V in a stirred 0.1 M phosphate buffer (pH 7.4, 10 mL); (2) sufficient UA (1 mM) was added into a stirred UOx-containing phosphate buffer (with known mass of Δm_{UOx}) of specific volume with its final concentration saturating the enzymatic reaction in the solution, and the change in the reduction current (Δi_c) on $(Au\text{-}PB)_{REd}$/Au disk electrode at -0.05 V in the sequent 60 s was recorded and used to quantify the enzymatically generated H_2O_2 ($n_{H_2O_2}$ here), according to the amperometric working curve obtained above. The evaluation of ESA_i was in a similar way, except that UOx-PABA-PtNPs bionanocomposite was used instead of native UOx.

In this work, the mass of added Δm_{UOx} for native and immobilized UOx (entrapped in the UOx-PABA-PtNPs bionanocomposite, a soluble sol) were both 0.075 mg. We obtained the Δi_c on $(Au\text{-}PB)_{REd}$/Au disk electrode at -0.05 V in the sequent 60 s as 0.45 and 0.31 μA for native and immobilized UOx (Fig. S5), respectively. Hence, the $n_{H_2O_2}$ could be calculated according to the calibration curve (Fig. S3, black curve), here was measured to be 0.122 μmol for native UOx and 0.084 μmol for immobilized UOx. So the values of ESA_n and ESA_i are calculated to be 1.63 U mg^{-1} and 1.12 U mg^{-1}, respectively.

Table S1. Electrochemical parameters for the two pairs of redox peaks of $(Au\text{-}PB)_{nano}$, $(Au\text{-}PB)_{REd}$, and PB_{con} modified EQCM Au electrodes given in Fig. 1*

Modified EQCM Au electrodes	E_{pa1} / V vs. SCE	i_{pa1} / mA	E_{pc1} / V vs. SCE	i_{pc1} / mA	ΔE_{p1} / V vs. SCE	E_{pa2} / V vs. SCE	i_{pa2} / mA	E_{pc2} / V vs. SCE	i_{pc2} / mA	ΔE_{p2} / V vs. SCE
$(Au\text{-}PB)_{nano}$	0.161	0.212	0.135	-0.289	0.026	0.901	0.0798	0.827	-0.0687	0.074
$(Au\text{-}PB)_{REd}$	0.164	0.482	0.136	-0.583	0.028	0.903	0.190	0.828	-0.177	0.075
PB_{con}	0.221	1.30	0.135	-2.52	0.086	0.928	0.181	0.801	-0.165	0.127

*The background currents are corrected.

Table S2. Performance comparison between the reported UA amperometric biosensors based on UOx and our UA biosensors*

Biosensor	Detection potential / V	Sensitivity / μA mM^{-1} cm^{-2}	LOD / μM	Linear range	Reference
Pt/$(PAA/PVS)_2PAA/(UOx/PAA)_9UOx$	0.6[b]	–	–	1 μM - 1 mM	1
uricase/Ir-C electrode	0.6[b]	110.7	10	0.1 mM - 0.8 mM	2
UOx/PB/CS/ITO	0.2[a]	–	0.18	5 μM - 1.15 mM	3
uricase/BS^3/APTES/ITO electrode	0.26[b]	39.35	37	50 μM - 0.58 mM	4
UOx-Th-SWNTs/GCE	-0.4[a]	90	0.5	2 μM - 2 mM	5
uricase/AuNP/MWCNT/Au	0.4[b]	–	10	10 μM - 0.8 mM	6
GNP/uricase/Au electrode	0.6[a]	108	7	20 μM - 2.5 mM	7
uricase/PBNPs/MWCNT/PANI/Au	0.4[b]	–	5	5 μM - 0.8 mM	8
CS/uricase-PTBA-Pt_{nano}/Pt_{plate}/Au	0.55[a]	134.4	1	5 μM -1.18 mM	9
SPE-PB-UOx biosensor	-0.05[b]	–	10	30 μM - 0.3 mM	10
CS/UOx-PABA-$Pt_{nano}/(Au\text{-}PB)_{REd}$/Au	-0.05[a]	247	0.1	0.2 μM - 0.25 mM	This work
CS/UOx-PABA-$Pt_{nano}/(Au\text{-}PB)_{nano}$/Au	-0.05 [a]	210	0.15	0.25 μM - 0.25 mM	This work
CS/UOx-PABA-Pt_{nano}/PB_{con}/Au	-0.05 [a]	185	0.2	0.3 μM - 0.2 mM	This work
CS/UOx-PABA-Pt_{nano}/Au	-0.05 [a]	–	–	–	This work
CS/UOx-PABA-$Pt_{nano}/(Au\text{-}PB)_{REd}$/Au	0.7[a]	223	0.2	0.3 μM - 0.65 mM	This work
CS/UOx-PABA-$Pt_{nano}/(Au\text{-}PB)_{nano}$/Au	0.7[a]	216	0.2	0.3 μM - 0.65 mM	This work
CS/UOx-PABA-Pt_{nano}/PB_{con}/Au	0.7[a]	174	0.25	0.5 μM - 0.6 mM	This work
CS/UOx-PABA-Pt_{nano}/Au	0.7 [a]	205	0.2	0.3 μM - 0.6 mM	This work

*The potential is cited versus (a) SCE or (b) Ag/AgCl reference electrode. PAA : poly(allylamine); PVS: poly(vinyl sulfate); Ir-C: Ir-modified carbon; BS^3: bis[sulfosuccinimidyl]suberate; APTES: 3-aminopropyltriethoxysilane; ITO: indium-tin-oxide; th: thionine; SWNTs: single-walled carbon nanotube; GCE: glassy carbon electrode; AuNP/GNP: gold nanoparticle; MWNT: multi-walled carbon nanotube; PBNPs: Prussian blue nanoparticles; PANI: polyaniline; PTBA: poly(thiophene-3-boronic acid); SPE: screen-printed electrode. Here, in the writing form of a modified electrode we take the following common standard. From right to left is in turn substrate electrode and gradually modified materials, thus the more to the left the more to the outer surface of electrode; "/" means interface (modification of an outer layer on the existing layer at the electrode) and "-" is used to delimit various individual components exiting in a composite.

1

Table S3. Determination of UA in human serum samples using the developed method*

Sample	Determined / μM	Spiked / μM	Found / μM	Recovery / %	RSD / %
Serum #1	253	20	20.6	103	2.3
		25	24.5	98	
		30	28.7	95.6	
Serum #2	226	20	20.4	102	4.4
		25	25.7	103	
		30	28.5	95	
Serum #3	304	20	19.4	97	2.7
		25	25.3	101.2	
		30	28.9	96.3	

*The samples were analyzed with the CS/UOx-PABA-PtNPs/$(Au\text{-}PB)_{REd}$/Au disk electrode. Recovery was obtained by adding standard solutions of UA to human serum samples which were 10-fold diluted with 0.1 M phosphate buffer (pH 7.4). The current response was recorded at -0.05 V vs SCE and each value is the mean of three determinations.

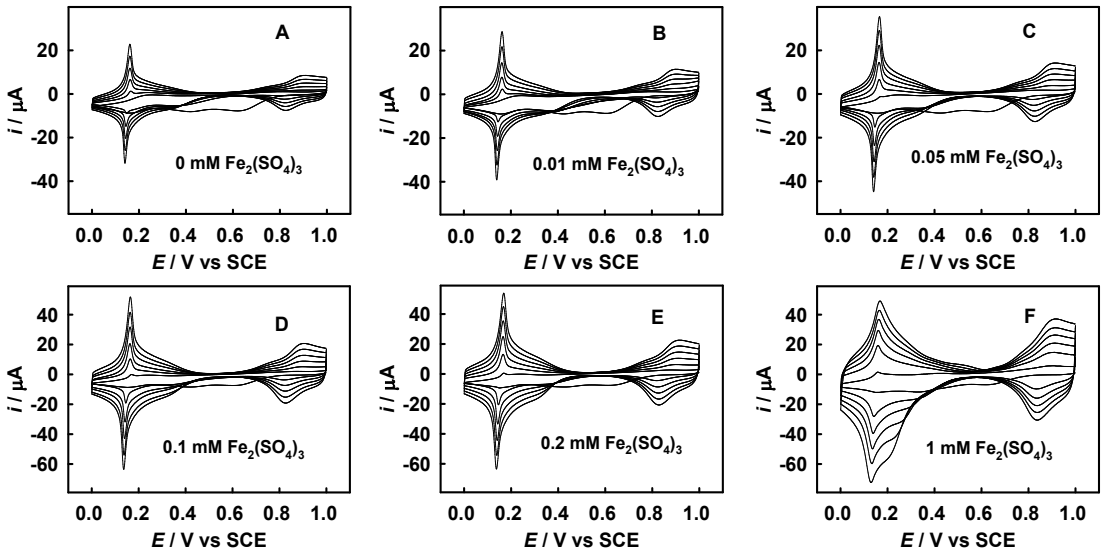

Fig. S1. Effect of concentration of the added $Fe_2(SO_4)_3$ on the electrodeposition of $(Au\text{-}PB)_{REd}$ film. Cyclic voltammograms (25 cycles in total) were obtained on the Au disk electrode in aqueous solutions of 1 mM $K_3Fe(CN)_6$ + 1 mM $HAuCl_4$ + 0.1 M K_2SO_4 containing 0 (A), 0.01 mM (B), 0.05 mM (C), 0.1 mM (D), 0.2 mM (E), and 1 mM $Fe_2(SO_4)_3$ (F), respectively. Scan rate: 50 mV s^{-1}. Initial potential: 1 V; Initial scan: negative. Only the cyclic voltammograms of the 1st, 5th, 10th, 15th and 25th cycles are shown for drawing clarity. Here, with the increase of $Fe_2(SO_4)_3$ concentration, the peak current after the 25-cycle CV electrodeposition gradually increased and became almost maximum after 0.1 mM $Fe_2(SO_4)_3$ was added. When the concentration of added $Fe_2(SO_4)_3$ was larger than 0.1 mM, the redox peaks near 0.2 V became notably wider due to the overlapping of the shoulder peaks and showed increased peak-to-peak separation. Since a faster electrode process should possess the sharper redox peaks, we believe that the addition of 0.1 mM $Fe_2(SO_4)_3$ can lead to an $(Au\text{-}PB)_{REd}$ film with the highest electrochemical reversibility and thus the best electrocatalytic efficiency, as confirmed in Figs. S2 and S3.

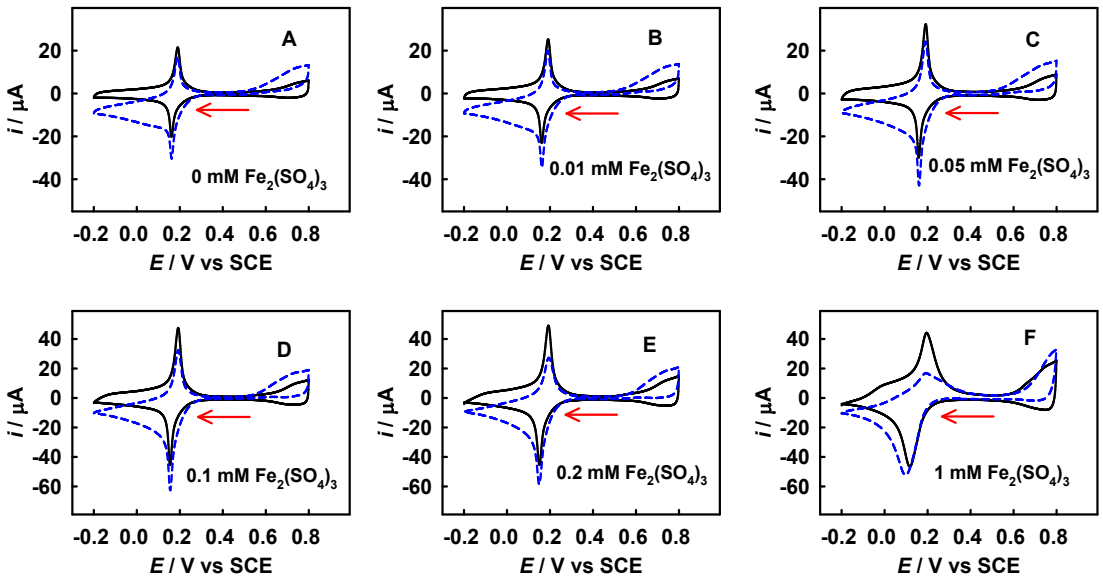

Fig. S2. Cyclic voltammograms at the above-prepared $(Au\text{-}PB)_{REd}$/Au disk electrodes (as shown in Fig. S1) in 0.1 M phosphate buffer (pH 7.4) with (blue dashed curve) and without (black solid curve) 1 mM H_2O_2. Scan rate: 50 mV s^{-1}. Initial potential: 0.35 V; Initial scan: negative. Here, the peak shape located at ca. 0.2 V remained almost the same as that of the 25th cycle electrodeposition curve in each case. After adding 1 mM H_2O_2, the oxidation current decreased and the reduction current increased, corresponding to the well-known electrocatalytic characteristic in CV experiments. The increment of the reduction peak current became maximum ($|\Delta i_{pc}|$ = 61.5 μA – 44.6 μA = 16.9 μA, background-corrected) when the concentration of added $Fe_2(SO_4)_3$ was 0.1 mM, demonstrating the greatest electrocatalytic efficiency for reduction of H_2O_2 here.

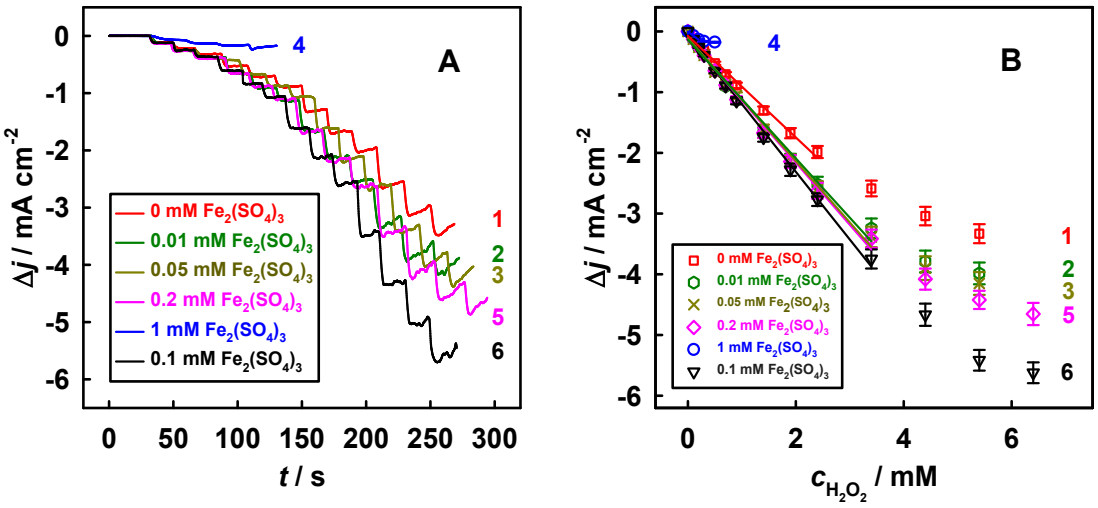

Fig. S3. Chronoamperometric responses (A) to successive additions of H_2O_2 and calibration curves (B) on the above-prepared $(Au\text{-}PB)_{REd}$/Au disk electrodes (as shown in Fig. S1) at -0.05 V (optimized) in 0.1 M phosphate buffer (pH 7.4). Here, the linear regression equations are Δj (mA cm^{-2}) = -0.736c (mM) - 0.699 (r^2=0.993) (case 1), Δj (mA cm^{-2}) = -0.976c (mM) - 0.135 (r^2=0.987) (case 2), Δj (mA cm^{-2}) = -1.01c (mM) – 0.106 (r^2=0.992) (case 3), Δj (mA cm^{-2}) = -0.665c (mM) - 0.0008 (r^2=0.999) (case 4), Δj (mA cm^{-2}) = -1.02c (mM) - 0.110 (r^2=0.993) (case 5), and Δj (mA cm^{-2}) = -1.11c (mM) - 0.0.077 (r^2=0.996) (case 6). The sensitivity of $(Au\text{-}PB)_{REd}$/Au disk electrode for amperometric detection of H_2O_2 (1.11 mA cm^{-2} mM^{-1}, case 6) is the largest, being approximately 1.5 times of that of $(Au\text{-}PB)_{nano}$/Au disk electrode (0.736 mA cm^{-2} mM^{-1}, case 1), demonstrating the excellent electrocatalytic efficiency of our $(Au\text{-}PB)_{REd}$ nanocomposite film. The H_2O_2-detection sensitivity of our $(Au\text{-}PB)_{REd}$/Au electrode is also superior to those of many reported H_2O_2 amperometric sensors [11-12].

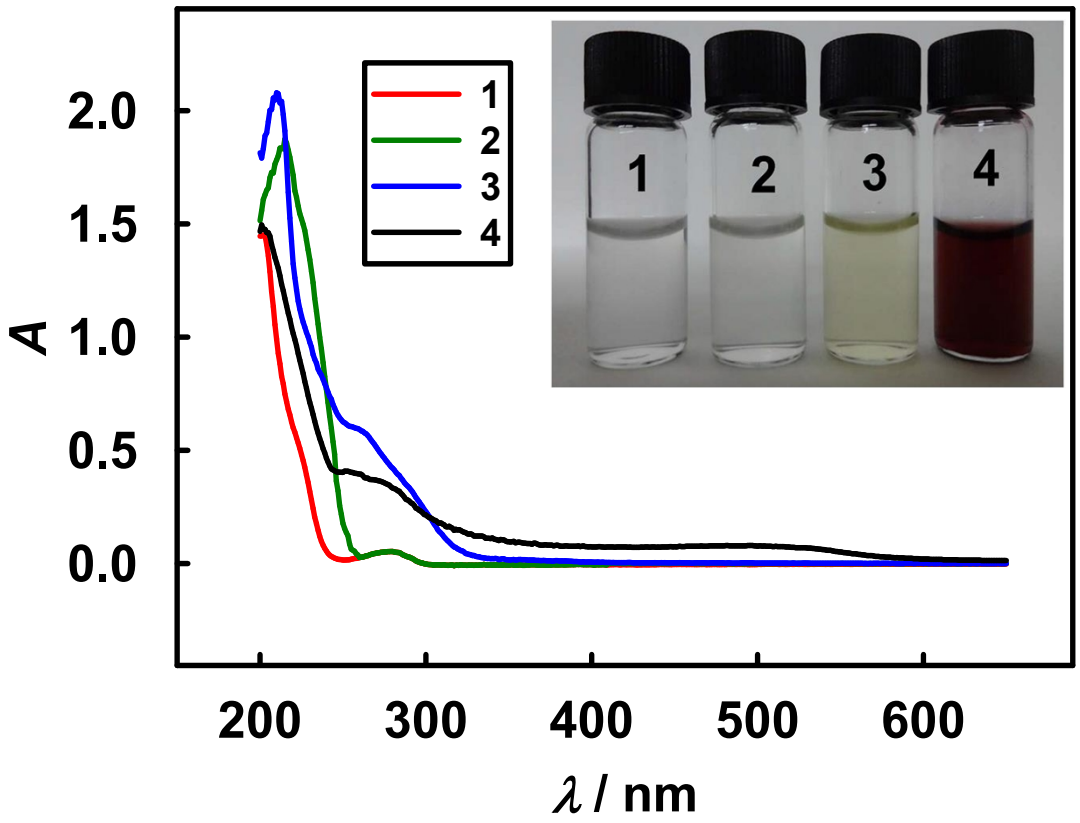

Fig. S4. UV-vis absorption spectra of UOx (1), UOx + ABA (2) after Na_2PtCl_6 was added to allow redox reaction at 35 °C for 0 (3) and 5 h (4) in 0.1 M phosphate buffer (pH 7.4). Inset: corresponding digital images of respective aqueous solution. Here, the absorption band at ca. 280 nm is assigned to the absorption of UOx in the phosphate buffer [13-14]. The absorption from ca. 200 to 260 nm increased after adding ABA. The absorption from ca. 200 to 300 nm decreased but the absorption from ca. 300 to 600 nm increased after adding Na_2PtCl_6 to allow reaction for 5 h at 35 °C, and the liquid mixture showed red color with some black precipitates, due to the coexistence of black polyaniline-like PABA precipitates, black Pt nanoparticles, and soluble oligomers of ABA in red color [9].

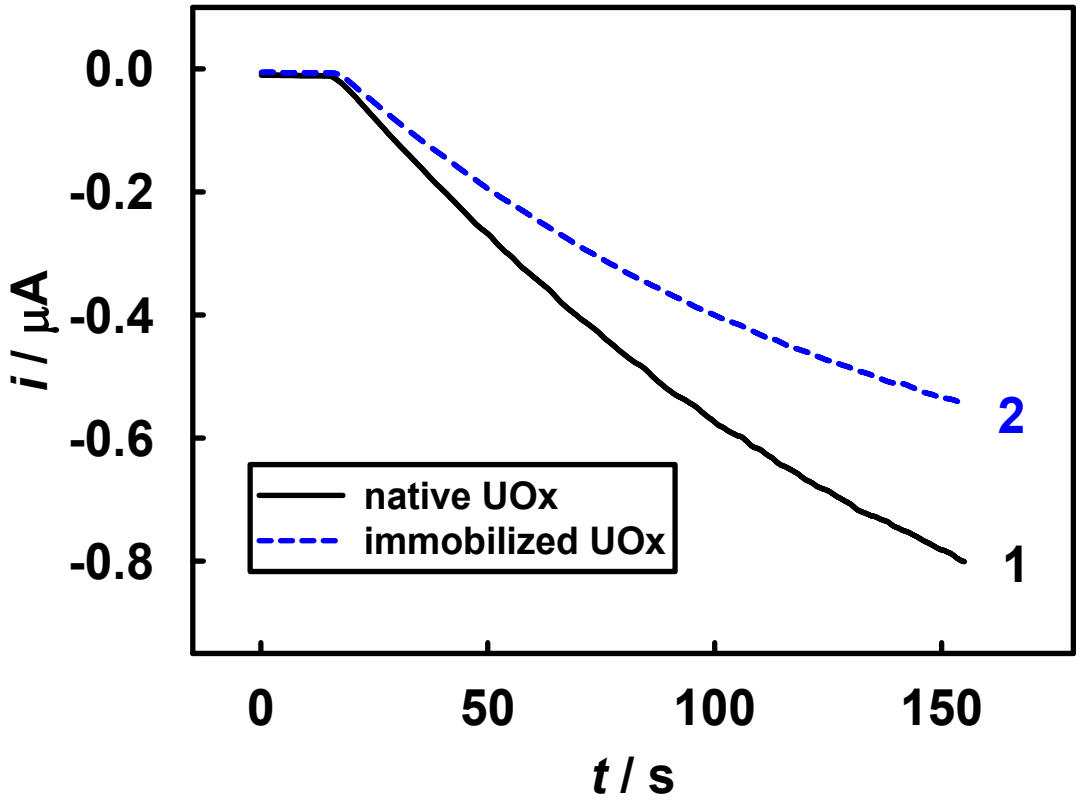

Fig. S5. Chronoamperometric responses of enzymatic kinetic of native (1) and immobilized (entrapped in UOx-PABA-PtNPs bionanocomposite, 2) UOx on $(Au\text{-}PB)_{REd}$/Au disk electrodes at -0.05 V to addition of 1 mM UA in 0.1 M phosphate buffer (pH 7.4).

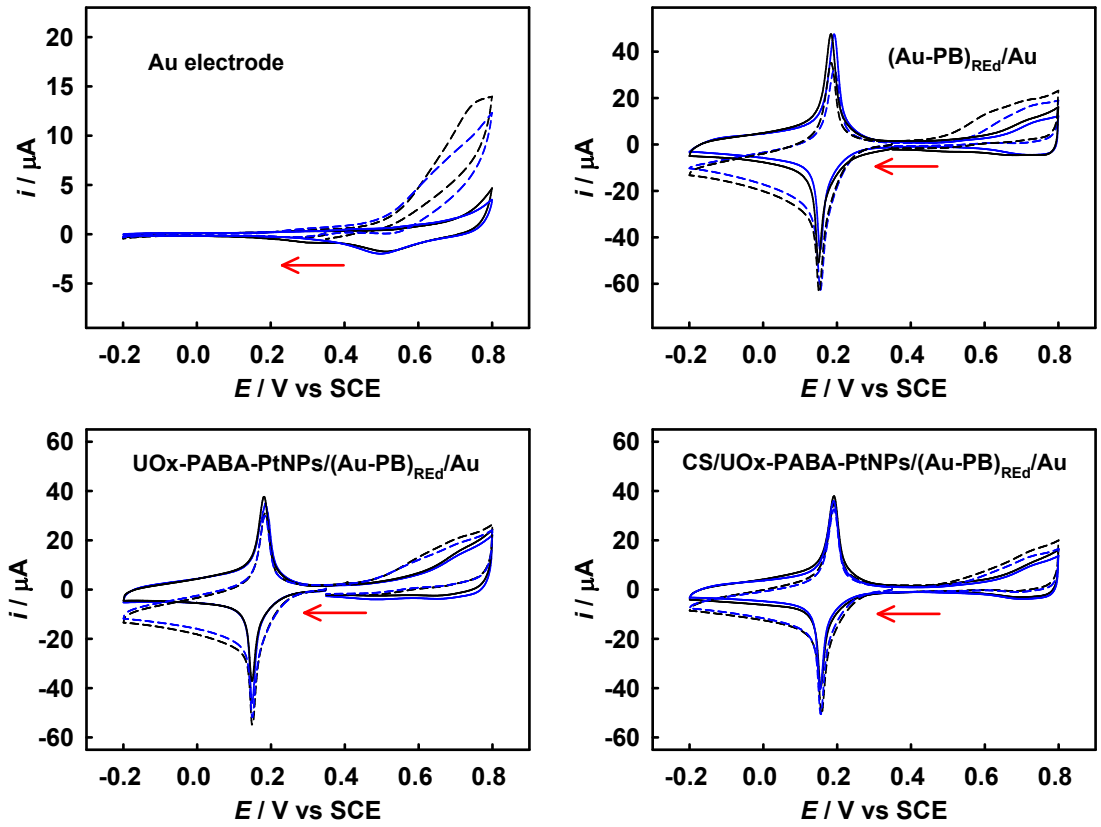

Fig. S6. Cyclic voltammograms at bare Au, $(Au\text{-}PB)_{REd}/Au$, UOx-PABA-PtNPs/$(Au\text{-}PB)_{REd}/Au$ and CS/UOx-PABA-PtNPs/$(Au\text{-}PB)_{REd}/Au$ disk electrodes in air saturated (black curves) or nitrogen saturated (blue curves) 0.1 M phosphate buffer (pH 7.4) with (dashed curves) or without (solid curves) 1 mM H_2O_2. Scan rate: 50 mV s^{-1}. Initial potential: 0.35 V; Initial scan: negative.

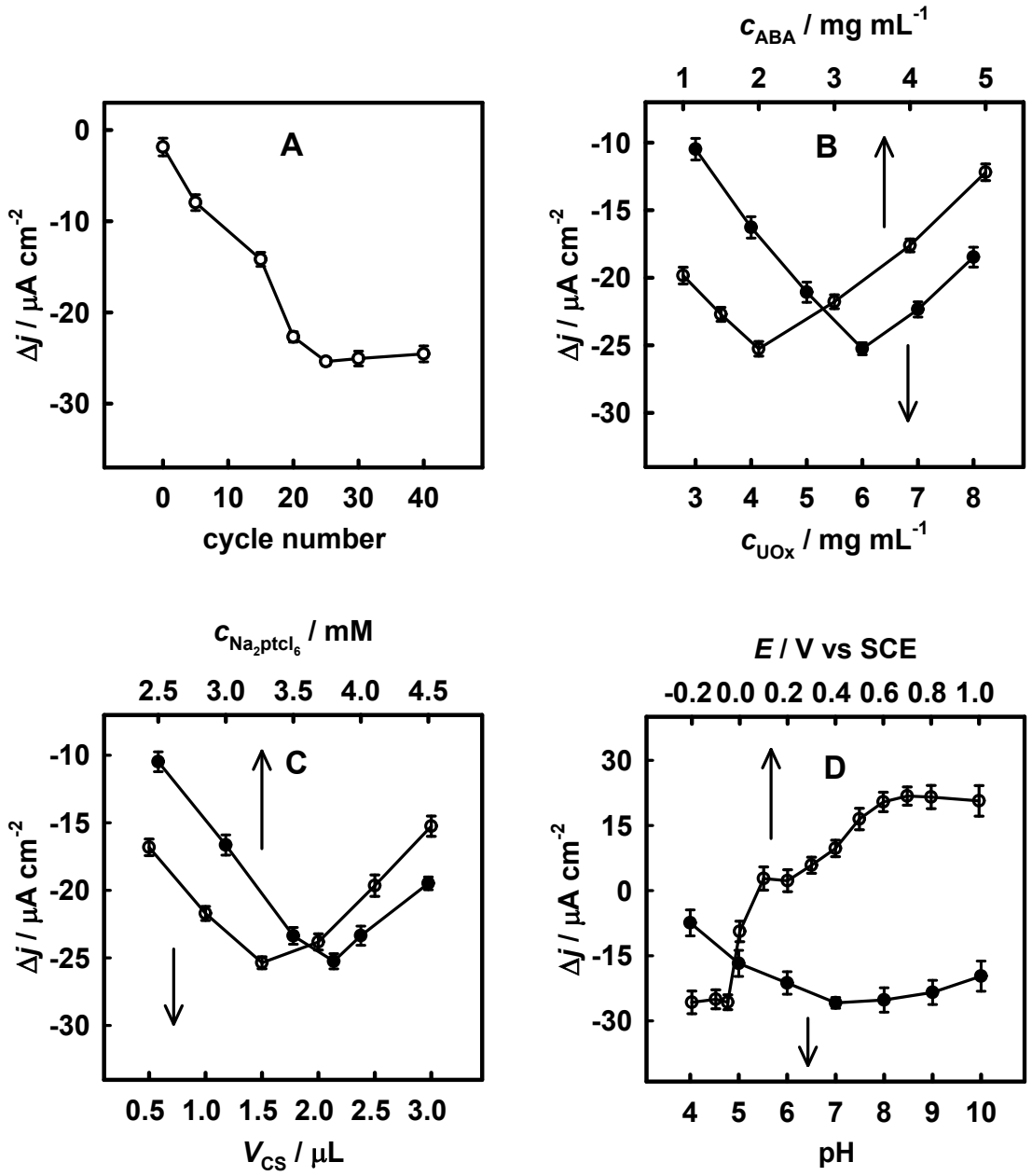

Fig. S7. Effects of CV cycle-number for electrodeposition of the $(Au\text{-}PB)_{REd}$ film on Au disk electrode (A), as well as the amounts of UOx (B), ABA (B), Na_2PtCl_6 (C) and CS (C) for preparing the CS/UOx-PABA-PtNPs/$(Au\text{-}PB)_{REd}$/Au disk enzyme electrode. Effects of solution pH (at -0.05 V vs SCE, D) and applied potential (D) on the steady-state current response of the CS/UOx-PABA-PtNPs/$(Au\text{-}PB)_{REd}$/Au disk electrode during biosensing in 0.1 M phosphate buffer containing 0.1 mM UA. Here, the thickness of $(Au\text{-}PB)_{REd}$ film was optimized to be 25 cycles, due probably to the fact that a thinner film gives insufficient active sites for the electrocatalyzed reduction of the enzymatically generated H_2O_2 and thus a

saturated response can be obtained after 25 CV cycles. The amount of the enzyme cast on electrode is a vital factor affecting the analytical performance of the biosensor and a maximum Δi value was found at 6 mg mL^{-1} UOx. Here, the excess ABA (2 mg mL^{-1}) can sufficiently reduce Na_2PtCl_4 (3.8 mM) to produce more PtNPs for increased biosensing sensitivity and the cast volume of 0.20 wt% CS was optimized as 1.5 μL. During biosensing of the prepared enzyme electrode, the maximum response was observed at 0.7 V (H_2O_2-oxidation mode) and at -0.05 V (H_2O_2-reduction mode) which are consistent with the early reports [7, 10]. The strongest boronic acid/diol complexes are generated at pH generally above the pK_a of boronic acid (8.9 for ABA) [15], but PB is not so stable at alkaline pH. Thus, the optimum pH was selected at physiological pH 7.4, which also makes it more efficient in quantitative determination of UA in biological fluids like human serum.

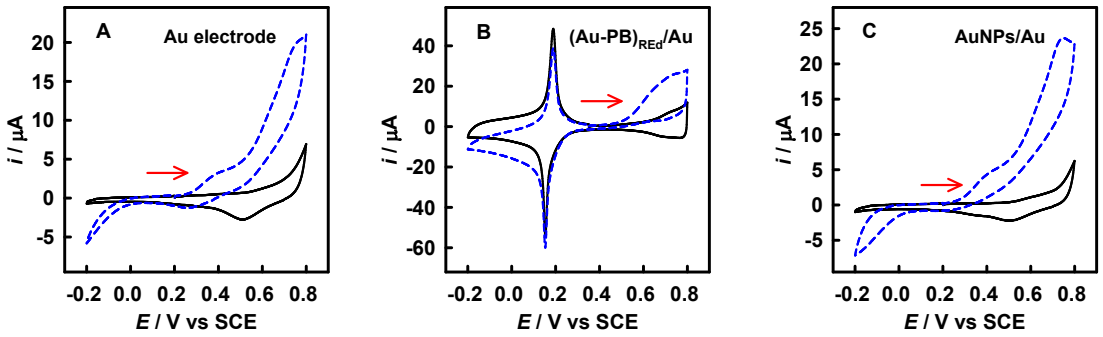

Fig. S8. Cyclic voltammograms of bare Au (A), $(Au\text{-}PB)_{REd}/Au$ (B) and AuNPs/Au (C, after removing PB by careful washing with 0.1 M NaOH and then HCl) disk electrodes in 0.1 M phosphate buffer (pH 7.4) with (blue dashed curves) or without (black solid curves) 1 mM H_2O_2. Scan rate: 50 mV s^{-1}. Initial potential: 0.2 V (except for B which is 0.35 V); Initial scan: positive. Here, the irreversible electrooxidation peak of H_2O_2 on the three electrodes occurred at a similar potential (ca. 0.7 V vs SCE). The peak current followed the order $(Au\text{-}PB)_{REd}/Au$ (24.3 μA) ≈ AuNPs/Au (24.2 μA) > bare Au (20.2 μA) disk electrode, thus we can come to the conclusion that the improved electrooxidation of H_2O_2 at $(Au\text{-}PB)_{REd}/Au$ disk electrode is due to the presence of AuNPs in the $(Au\text{-}PB)_{REd}$ film. In addition, it is well known that the electrooxidation of H_2O_2 on a Pt electrode is easier (at a lowered overpotential) than that on an Au electrode, as a result of the enhanced catalytic ability toward electrooxidation of H_2O_2 intrinsically on Pt [16-17]. However, in our cases, (1) no obvious characteristic current peaks of Pt were observed on the CV curves of UOx-PABA-PtNPs/$(Au\text{-}PB)_{REd}/Au$ and CS/UOx-PABA-PtNPs/$(Au\text{-}PB)_{REd}/Au$ disk electrodes (the cathodic peak of Pt oxides and dissolved oxygen is generally at ca. 0.3 V on a Pt electrode in 0.1 M H_2SO_4 [18]), probably due to the shielding of the large redox peaks of PB, as shown in Fig. S6; (2) from the effect of applied potential on the steady-state current response of the CS/UOx-PABA-PtNPs/$(Au\text{-}PB)_{REd}/Au$ disk electrode during biosensing in 0.1 M phosphate buffer (pH 7.4) containing 0.1 mM UA (Fig. S7 D), a saturated response current was obtained at 0.7 V vs. SCE, which is more positive than the typical results reported on Pt electrodes (generally on ca. 0.55 V vs. SCE[9,19]). The above results and discussion support that the PtNPs here cannot exhibit notable electroactvity and electrocatalytic activity for oxidation of H_2O_2 under our experimental

conditions, as explained below. Unlike the cases of electrodeposited PtNPs, the chemically generated PtNPs here should be mostly embedded in the bionanocomposite, and most of them should not be electrically connected to the electrode after cast-coating the PtNPs-containing bionanocomposite on the electrode surface to exhibit obvious electroactivity and electrocatalysis activity, and only a few PtNPs residing on the outer surfaces of bionanocomposite particles can be electrically connected to the electron-conducting Au sites of $(Au\text{-}PB)_{REd}$ to exhibit notable electroactvity and electrocatalytic activity for oxidation of H_2O_2 (note that the PB sites of $(Au\text{-}PB)_{Red}$ is not electron-conducting). Hence, we conclude that the improved electrooxidation of H_2O_2 even at the CS/UOx-PABA-PtNPs/$(Au\text{-}PB)_{REd}$/Au disk enzyme electrode is predominantly due to the presence of AuNPs in the $(Au\text{-}PB)_{REd}$ film, and we also believe that the PtNPs here can contribute to the improved analytical performance of our enzyme electrode to a small degree.

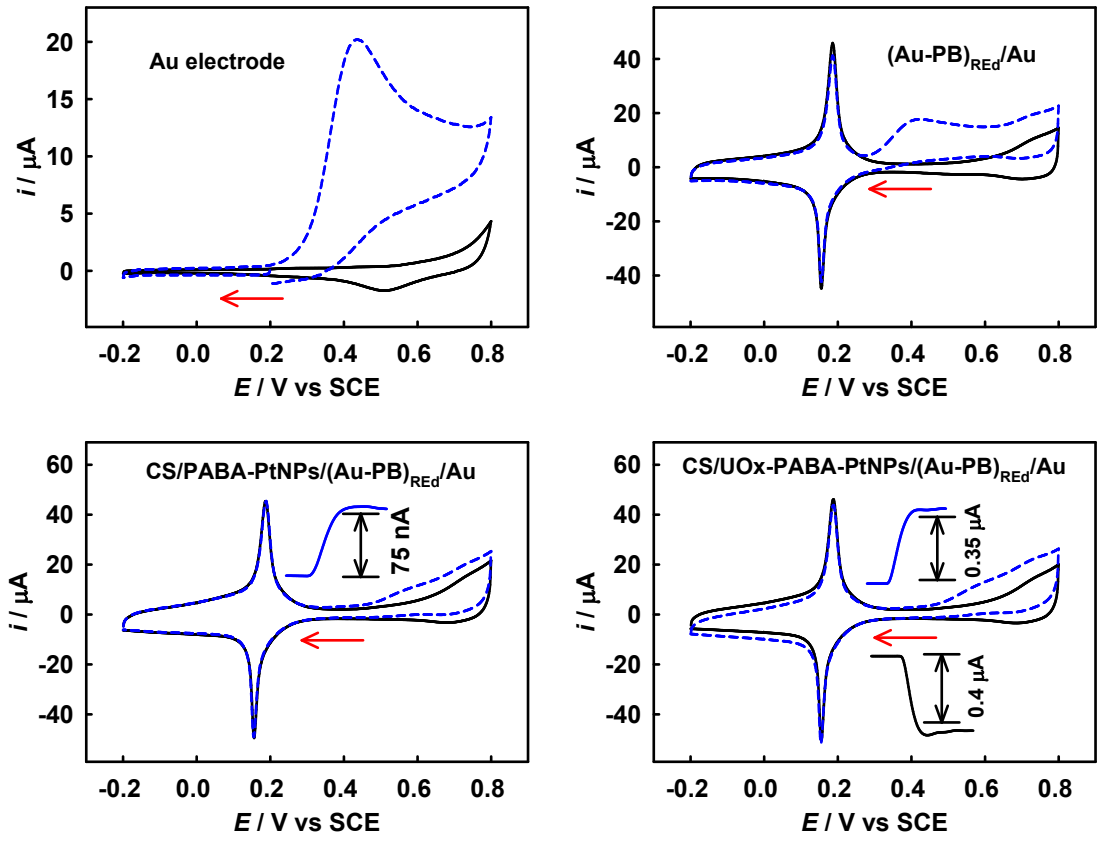

Fig. S9. Cyclic voltammograms at bare Au, $(Au\text{-}PB)_{REd}/Au$, CS/PABA-PtNPs/$(Au\text{-}PB)_{REd}$/Au and CS/UOx-PABA-PtNPs/$(Au\text{-}PB)_{REd}$/Au disk electrodes in 0.1 M phosphate buffer (pH 7.4) with (blue dashed curves) or without (black solid curves) 2 mM UA. Scan rate: 50 mV s^{-1}; Initial potential: 0.35 V (except for the bare Au disk electrode which is 0.2 V); Initial scan: negative. Inset: amperometric responses to 50 µM UA at 0.7 V (H_2O_2-oxidation mode, blue curves) and -0.05 V (H_2O_2-reduction mode, black solid curve) in 0.1 M phosphate buffer (pH 7.4).

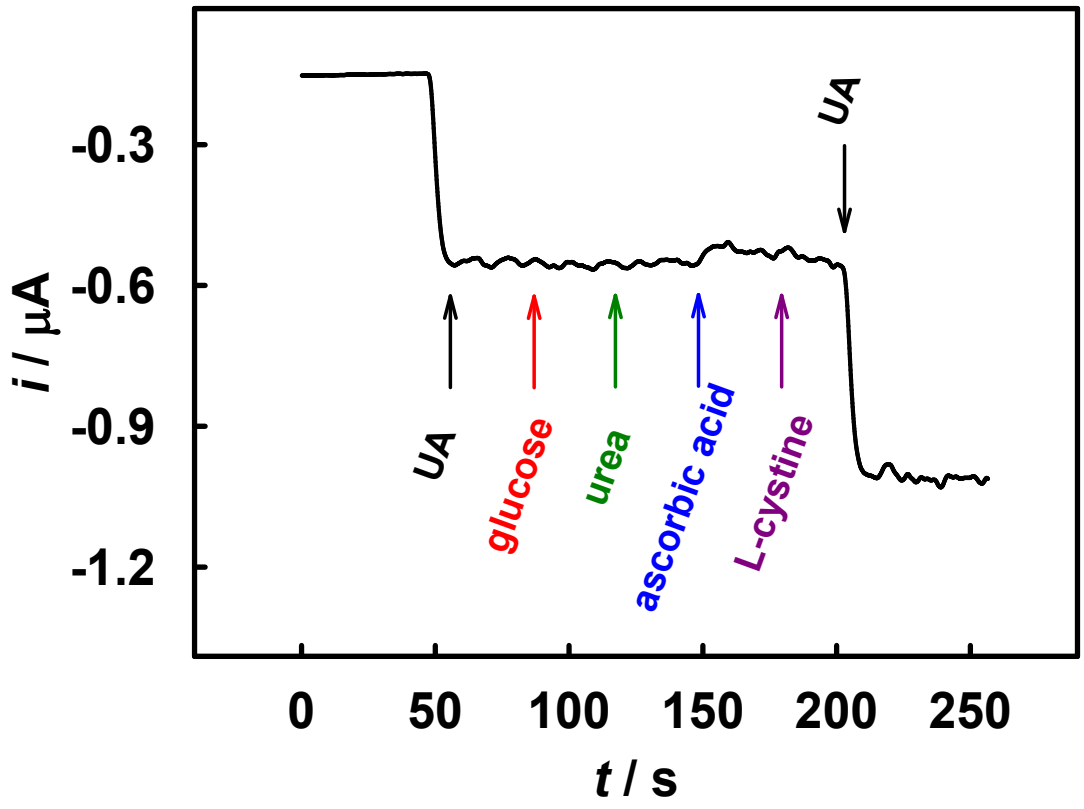

Fig. S10. Effects of additions of 0.1 mM UA, 1 mM glucose, 1 mM urea, 0.1 mM ascorbic acid, 0.1 mM L-cystine, and 0.1 mM UA on the response of CS/UOx-PABA-PtNPs/(Au-PB)$_{REd}$/Au disk electrode at -0.05 V in 0.1 M phosphate buffer (pH 7.4).

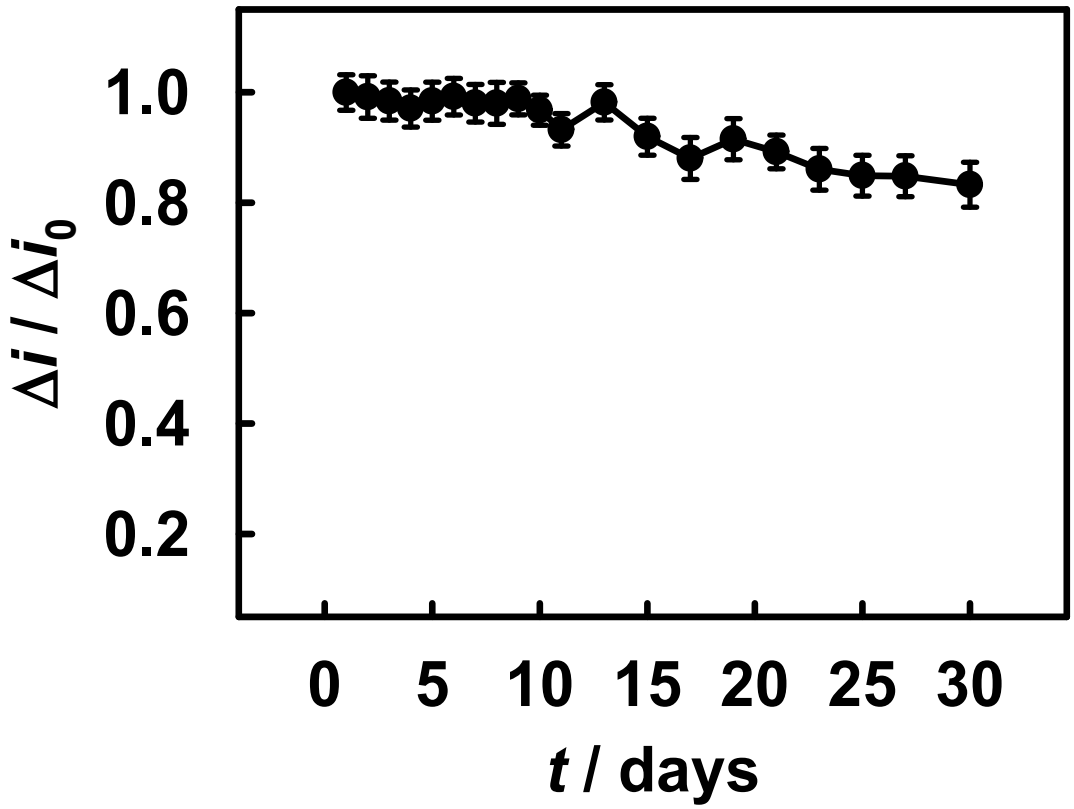

Fig. S11. The storage stability of the constructed biosensor under storage conditions (in a refrigerator at 4 °C). The measurements were conducted in 0.1 M phosphate buffer (pH 7.4) containing 50 μM UA at -0.05 V vs SCE.

References (The numbering here is only for the Supporting Information)

1 T. Hoshi, *Talanta,* 2003, **61**, 363-368.

2 Y. C. Luo, J. S. Do and C. C. Liu, *Biosens. Bioelectron.,* 2006, **22**, 482-488.

3 H. Tao, X. Wang, X. Wang, Y. Hu, Y. Ma, Y. Lu and Z. Hu, *J. Nanosci. Nanotechnol.,* 2010, **10**, 860-864.

4 T. Ahuja, Rajesh, D. Kumar, V. K. Tanwar, V. Sharma, N. Singh and A. M. Biradar, *Thin Solid Films,* 2010, **519**, 1128-1134.

5 D. Chen, Q. Wang, J. Jin, P. Wu, H. Wang, S. Yu, H. Zhang and C. Cai, *Anal. Chem.,* 2010, **82**, 2448-2455.

6 N. Chauhan and C. S. Pundir, *Anal. Biochem.,* 2011, **413**, 97-103.

7 Y. Liu, M. Yuan, L. Liu and R. Guo, *Sens. Actuators B,* 2013, **176**, 592-597.

8 R. Rawal, S. Chawla, N. Chauhan, T. Dahiya and C. S. Pundir, *Int. J. Biol. Macromol.,* 2012, **50**, 112-118.

9 Y. Huang, L. Bu, W. Wang, X. Qin, Z. Li, Z. Huang, Y. Fu, X. Su, Q. Xie and S. Yao, *Sens. Actuators B,* 2013, **177**, 116-123.

10 S. Piermarini, D. Migliorelli, G. Volpe, R. Massoud, A. Pierantozzi, C. Cortese and G. Palleschi, *Sens. Actuators B,* 2013, **179**, 170-174.

11 M. Gaitan, V. R. Goncales, G. J. Soler-Illia, L. M. Baraldo and S. I. de Torresi, *Biosens. Bioelectron.,* 2010, **26**, 890-893.

12 G. Wang, J. Zhou and J. Li, *Biosens. Bioelectron.,* 2007, **22**, 2921-2925.

13 M. S. Caves, B. K. Derham, J. Jezek and R. B. Freedman, *Biochemistry,* 2013, **52**, 497-507.

14 H. Hamzah, Z. Zain, N. Musa, Y. Lin and E. Trimbee, *J. Anal. Bioanal. Tech.,* 2013, **7**, 2.

15 J. Yan, G. Springsteen, S. Deeter and B. Wang, *Tetrahedron,* 2004, **60**, 11205-11209.

16 R. D. O'Neill, S.-C. Chang, J. P. Lowry and C. J. McNeil, *Biosens. Bioelectron.,* 2004, **19**, 1521-1528.

17 S. B. Hall, E. A. Khudaish and A. L. Hart, *Electrochim. Acta,* 1997, **43**, 579-588.

18 Z. Huang, Y. Liu, F. Xie, Y. Fu, Y. He, M. Ma, Q. Xie and S. Yao, *Chem. Commun.,* 2012, **48**, 12106.

19 H. Tang, F. Yan, Q. Tai and H. L. W. Chan, *Biosens. Bioelectron.,* 2010, **25**, 1646-1651.